FULL PAPER

DOI: 10.1002/chem.200700872

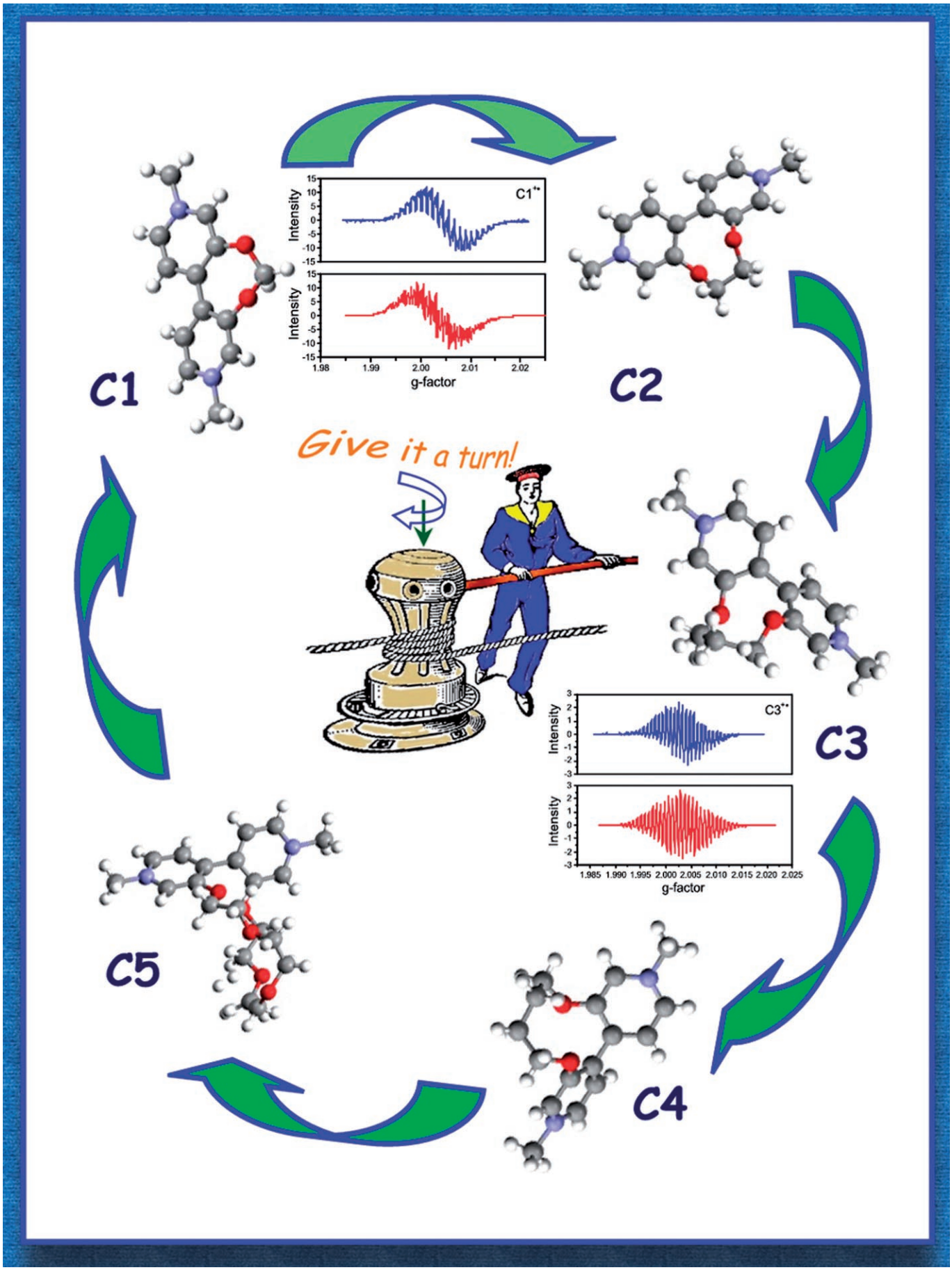

A Spectroscopic Study of the Reduction of Geometrically Restrained Viologens

Andrew C. Benniston,*[a] Anthony Harriman,*[a] Peiyi Li,[a] James P. Rostron,[a] Ross W. Harrington,[b] and William Clegg[b]

Abstract: A small series of *N*,*N*′-dimethyl-4,4′-bipyridinium dication derivatives (commonly known as viologens) has been synthesized and fully characterized; a short dialkoxy tether attached at the 3,3′-positions is used to alter the central dihedral angle. These angles were determined by both single-crystal X-ray diffraction and by computational studies made for the dication, radical cation, and neutral species in a solvent reservoir. The dihedral angle derived for the dication controls the first reduction potential, whereas the geometry of the resultant π-radical cation determines the magnitude of the second reduction potential. The optical absorption spectra recorded for the various species, and especially those of the radical cations, and the EPR spectral parameters of the π-radical cations also depend on the molecular geometry. In particular, the central dihedral angle influences the spin density distribution around the aromatic nucleus and, by way of comparison to the parent viologen, it has been possible to resolve the angle dependence from the inherent inductive effect of the strap. These results are considered in terms of the degree of electronic communication between the two aromatic rings, as controlled by the length of the tether.

Keywords: electrochemistry · electronic coupling · EPR spectroscopy · radicals · reduction

Introduction

The class of compounds based on *N*,*N*′-dialkyl-4,4′-bipyridinium cations, known commonly as the "viologens", have figured prominently in the chemical sciences for many decades.[1] Developed originally as herbicides,[2] viologen salts have been used extensively as electron relays in artificial photosynthetic systems[3] and as redox mediators in catalytic cycles.[4] More recently, viologen derivatives have played a key role in the development of molecular-scale devices,[5] often being incorporated into rotaxanes,[6] catenanes,[7] and cyclophanes.[8] A characteristic feature of all viologens is their facile one- and two-electron reduction, with the monocation being a highly colored and stable free radical.[9] The corresponding reduction potentials are relatively insensitive to the nature of the alkyl substituent but these are modulated markedly by substitution into the bipyridinium ring.[10] It is known that for the *N*,*N*′-dimethyl-4,4′-bipyridinium dication (methyl viologen, MV^{2+}) the dihedral angle at the connecting C–C bond is around 45° for the ground state, but this decreases to almost 0° upon one-electron reduction.[11] This planar geometry facilitates delocalization of the spin density across the molecule and is a critical feature of the redox chemistry of this family of compounds.

We now describe a small series of methyl viologen derivatives in which the central dihedral angle is constrained, at least in the ground state. This is accomplished by attaching a short tethering strap across the 3,3′-positions, with the length of the strap controlling the torsion angle between the connected *N*-methylpyridinium rings. It is shown that the redox and spectroscopic properties depend markedly on the length of the tether. These findings can be compared with the known "diquat" series of electron mediators in which the reduction potential is determined by the length of the dialkylating chain.[12] Our interest in such molecules stems from a general need to better understand the angular dependence for electronic coupling in donor–acceptor dyads.[13] In some respects, the viologen monocation can be considered as a simple analogue of organic mixed-valence

[a] Dr. A. C. Benniston, Prof. A. Harriman, Dr. P. Li, Dr. J. P. Rostron
Molecular Photonics Laboratory, School of Natural Sciences
University of Newcastle, Newcastle upon Tyne, NE1 7RU (UK)
Fax: (+44) 191-222-8660
E-mail: a.c.benniston@ncl.ac.uk
anthony.harriman@ncl.ac.uk

[b] Dr. R. W. Harrington, Prof. W. Clegg
Crystallography Laboratory, School of Natural Sciences
University of Newcastle, Newcastle upon Tyne, NE1 7RU, (UK)

Supporting information for this article is available on the WWW under http://www.chemeurj.org/ or from the author.

systems,[14] albeit with a closely coupled electronic system. It was shown recently[15] that hole transfer in mixed-valence, binuclear $Ru^{III/II}$ poly(pyridine) complexes was optimal when the dihedral angle of the bridging biphenyl unit approached 0°. These constrained viologen derivatives offer the possibility to examine how the electronic properties depend on geometry in a complementary manner. A further point for consideration relates to the possibility of modulating the reduction potential of a relatively simple compound by rapid switching of the conformation. Such materials would have important applications in molecular-scale optoelectronic devices.

Results and Discussion

Synthesis: Prior to our preliminary communication[16] reporting two constrained viologen derivatives, very few 3,3′-functionalized derivatives had been described in the literature. Rebek et al.[22] prepared 4,4′-binicotinic acid from 3-picoline by way of reductive coupling and oxidation, and used this approach to produce the corresponding cyclic anhydride. Sleegers and Dehmlow[23] prepared 3,3′-dimethoxy-4,4′-bipyridine by self-coupling of 3-methoxypyridine. This latter compound was used subsequently to synthesize the hydroxy analogue by demethylation under quite harsh conditions. We found an alternative strategy by which to prepare 4,4′-bipyridinyl-3,3′-diol by Suzuki coupling of two pyridine derivatives (Scheme 1). The idea was to link the two oxygen atoms of 4,4′-bipyridinyl-3,3′-diol via a suitable tether. Also shown in Scheme 1 is the attempted alternative method of carrying out an intramolecular coupling reaction which requires fewer synthetic steps.

The preparation of the viologen precursors **1a**–**1e** is as follows: starting from pyridin-3-ol, the known starting materials **2**, **3**, and **4** were prepared. Lithiation at the 4-position of **2** and reaction with $B(OiPr)_3$, followed by hydrolysis, gave **5** in 65% yield. It should be noted that reaction of **3** with **5** using standard Suzuki coupling conditions and work up afforded the monoprotected derivative **6** rather than the expected diprotected product. The basic workup conditions selectively remove only one of the carbamoyl protecting groups. This fortuitous result bodes well for selective functionalization of **6** with other groups. The final carbamoyl group was readily removed from **6** by using NaOH to afford **7** in a yield of 75%. Tethering reactions of **7** were performed by deprotonation of the hydroxy groups, followed by slow addition of either diiodomethane or ditosyloxyalkane/ether derivatives. The isolated yields of **1a**–**1e** were modest (9%-33%). Simple methylation of **1a**–**1e** with iodomethane followed by anion exchange with PF_6^- and recrystallization afforded the desired viologen analogues **C1**–**C5** as crystalline solids. Single-crystal structures were determined for derivatives **C1**–**C5** and confirm the structural assignments. There is only one example in the CSD of a structure with the methyl viologen unit with a connection of more than one atom between the 3,3′-positions for which geometrical results are available. This has a large and complex connector including a barium ion sandwiched by two crown ethers, and its torsion angle is 61.3°, which is the same as found for **C4**.[24]

As an alternative strategy, we were interested to see if intramolecular Ullmann coupling[25] could also be used to create strapped derivatives. The linking of 4-iodopyridin-3-ol **4** with bis(tolyl-4-sulfonyloxy)-propane afforded **8** in 60% yield. Intramolecular coupling of **8** using activated copper in DMF at 150°C proceeded smoothly, as evidenced by consumption of the starting material. However, isolation of pure **1c**, even by careful chromatography, was not possible, since it was always contaminated with the mono-iodo byproduct that arose from partial reduction of **8**. Thus, intramolecular cyclization does not look a feasible route by which to generate strapped 4,4′-bipyridine derivatives.

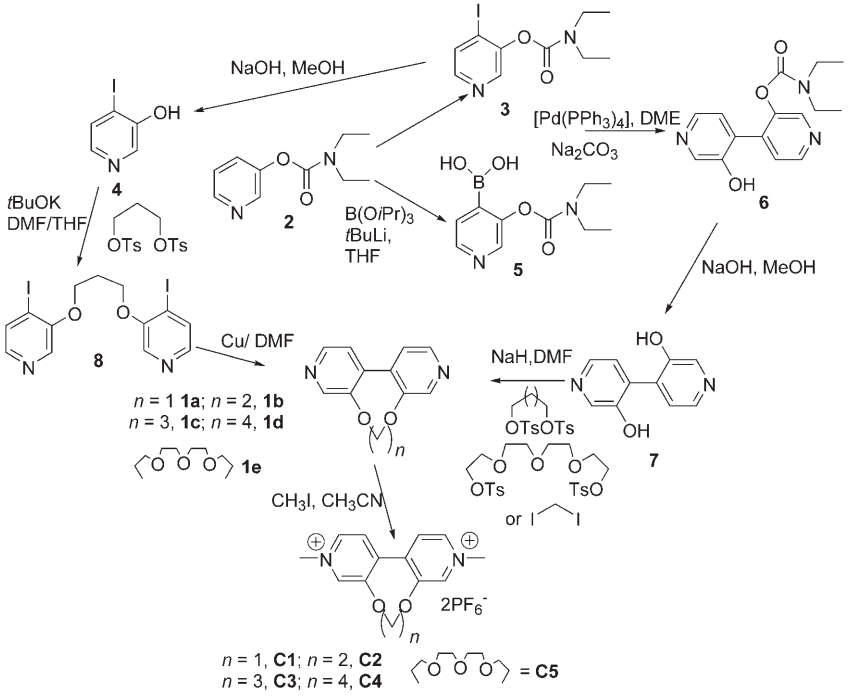

Scheme 1. Synthetic methods suitable for preparing the constrained methyl viologen derivatives.

Static structures for the ground-state molecules: Molecular modeling studies[26] indicate

that the isolated MV^{2+} dication is twisted, with a central dihedral angle (φ) of 44°. By comparison, crystal structures of $MV^{2+}X_2$ (in which X = Br^- or Cl^-) disclose the dication to be almost planar,[27] with no close intermolecular contacts within the unit cell. However, intermolecular interactions exist between the counterions and the N atoms due to electrostatic attractive forces. Ground-state molecular structures of **C1**–**C5** obtained by X-ray crystallographic analysis reveal a gradual alteration in the dihedral angle between the two pyridinium rings (Figure 1). Although these angles are influenced by the competing forces of crystal packing, repulsive intramolecular H–H interactions, and the drive towards planarity in order to increase π overlap,[28] the isomorphous nature of **C2**, **C3**, and **C4** means that they have essentially the same (or very similar) packing forces. Consequently, the trends exposed by such crystallographic data ought to follow through to the solution phase, although the actual details are likely to change. The main X-ray data are summarized in Table S1 given in the Supporting Information and, in addition to the central dihedral angles, include the H···H′ distances obtained after adjusting the C–H bond lengths to the expected value of 1.08 Å. The O···O distances are also provided. The molecular structure of **C1** clearly shows the molecule to be almost planar, with a measured dihedral angle (φ) of 12.2°. On moving from **C2** through **C4** the dihedral angle increases from 54.3° to 55.8° to 61.3°, respectively (Table S1). In the most flexible system (**C5**) the dihedral angle is reduced to 57.7°, which is probably because of additional crystal packing effects involving the polyether strap.

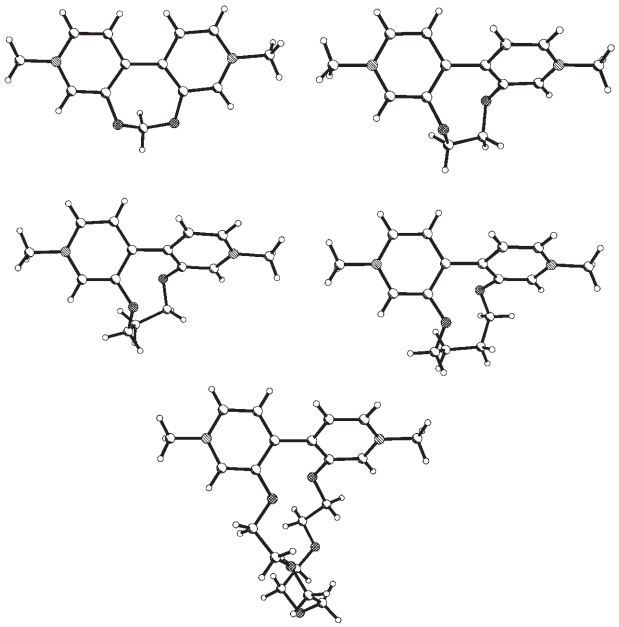

Figure 1. The structures of the dications of **C1**–**C5** determined by X-ray crystallography. Anions and minor disorder components are omitted. For each dication, the view is perpendicular to the left-hand pyridinium ring, so that the variation of torsion angles between the rings might be seen more readily.

Molecular modeling studies were made in an effort to identify the lowest energy conformations of the isolated molecules. Several such investigations[26] have been carried out previously for the parent viologen, by using a variety of computational methods and conditions, with the general conclusion that the central dihedral angle is between 40 and 50°. Our calculations, made at the B3LYP level[29] for MV^{2+} in a reservoir of acetonitrile molecules, indicate a dihedral angle of 43°, in agreement with most of the previous computations. The same calculations made for the sterically restricted viologens concluded that φ depends on the length of the constraining tether, but that this angle differs from that derived by X-ray crystallography (Table 1), especially for **C1**. Even so, the trend in φ values remains in good agreement with the results derived from the X-ray studies. In particular, the computed φ values show a large increase on going from **C1** to **C2** and only slight variations upon further extension of the strap length. The crown ether strap, which is considerably longer than the hydrocarbon-based tethers, imposes a dihedral angle that is closely comparable to that of **C4**. The computed bond lengths are of the order of 1.49 Å and exhibit only a slight dependence on the calculated dihedral angle. As expected, however, the way in which the strap packs into the available space controls the geometry around the connection and the largest dihedral angle is found for **C2**. It should be noted that, although there are clear variations in the central dihedral angle among these derivatives, the tethering strap also causes the molecule to bend slightly into a "banana" shape in order to relieve steric crowding.[30] The final structure includes contributions from both effects.

Table 1. Computed structural data for the geometrically restricted viologen derivatives.

	dication		monocation		neutral	
	φ [°]	R_{CC} [Å]	φ [°]	R_{CC} [Å]	φ [°]	R_{CC} [Å]
C1	35.7	1.481	10.1	1.404	1.7	1.363
C2	62.3	1.498	22.8	1.419	1.5	1.366
C3	51.3	1.488	25.3	1.424	5.6	1.365
C4	56.1	1.493	21.3	1.413	5.3	1.368
C5	54.1	1.492	21.1	1.415	10.5	1.384

Calculated structures for the reduced species: In agreement with earlier work,[26,31] our quantum chemical calculations predict that the one-electron reduced form of the parent viologen, $MV^{\bullet+}$, is essentially planar. The computed dihedral angle (φ) around the connecting C–C bond is only 1.3° while the length of this bond (R_{CC}) is calculated to be 1.417 Å. On further reduction to the neutral species, MV, there is a slight decrease in the dihedral angle (φ = 0.2°) and a modest modulation of the bond length (R_{CC} = 1.366 Å). This bond length, when compared to that determined for MV^{2+} (R_{CC} = 1.464 Å), can be used to suggest that the reduced species shows increased electron delocalization by taking on more double-bond character at the linkage. The

decreased dihedral angle found for $MV^{\bullet+}$ indicates that the drive to delocalize the charge overcomes the modest stereochemical crowding caused by the clashing hydrogen atoms. For the strapped analogues, one-electron reduction causes a decrease in both φ and R_{CC} (Table 1). These derivatives cannot attain planar geometries because of the bulky strap, but it is clear that the π-radical cation attempts to minimize φ and that the derived values represent a compromise between steric repulsion and increased conjugation. In each case, one-electron reduction is accompanied by a decrease in φ by at least 20°. Again, the largest dihedral angle is found for **C2** and the smallest for **C1**, such that adding this extra methylene group has a profound effect on the molecular geometry. Under the same conditions, there is a marked decrease in R_{CC} relative to the corresponding dication, with the actual values remaining comparable throughout the series. There is, however, a small correlation between φ and R_{CC} (Table 1) as computed for the π-radical cations.

The neutral species, as formed upon addition of two electrons, attempts to adopt a planar geometry, with φ values ranging between 0 and 10° (Table 1). In each case, there is a decrease in the relevant R_{CC} values, which tend towards 1.37 Å, as the molecule attempts to maximize electron delocalization by forming a central double bond. This behavior is similar to that reported earlier[26] for the parent viologen, as noted above. There is no clear relationship between φ values derived for the dication and the neutral species, and as a consequence it is difficult to rationalize the computed structures in terms of the strap length. An evident limitation of these calculated geometries is that they refer to the lowest-energy conformations, but it is realized that the structures will be in dynamic motion in solution at ambient temperature. The central dihedral angles, in particular, are likely to fluctuate quite considerably due to thermal motions and such behavior might obscure any weak correlation between geometry and electronic properties. This likelihood was addressed by way of molecular dynamics simulations and temperature-dependent NMR studies.

Molecular dynamics: The ^{1}H NMR spectra recorded for **C1**–**C5** display typical aromatic resonances associated with the viologen unit. Closer inspection of proton resonances due to the constraining bridge reveals more insight into restricted ring-ring rotation dynamics. As an example, selected variable temperature ^{1}H NMR spectra are shown for **C2** in CD_3CN (Figure 2). At room temperature, the ^{1}H NMR spectrum (not shown) displays only a broad signal at approximately 4.6 ppm, which corresponds to the methylene units of the bridge. Upon cooling the sample to 273 K, two broad signals emerge at about 4.7 and 4.2 ppm, respectively. Further cooling results in these signals developing into two well-resolved doublets. Similar dynamic NMR behavior has been noted for analogous conformationally-restricted 2,2′-biphenol-based assemblies,[32] for which the existence of atropisomers was speculated. A more comprehensive examination of this phenomenon was attempted using molecular dynamics simulations (MDS) made for **C1**–**C5**.

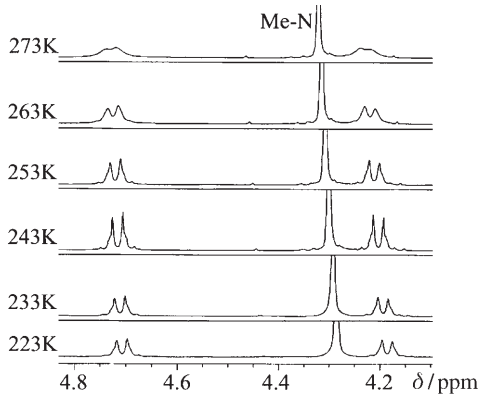

Figure 2. Variable-temperature ^{1}H NMR spectra recorded for **C2** in CD_3CN.

MDS runs conducted for the dications showed that the central dihedral angle varied significantly about the mean value computed for the lowest energy conformation (Figure 3). In fact, φ oscillated over a range of angles cover-

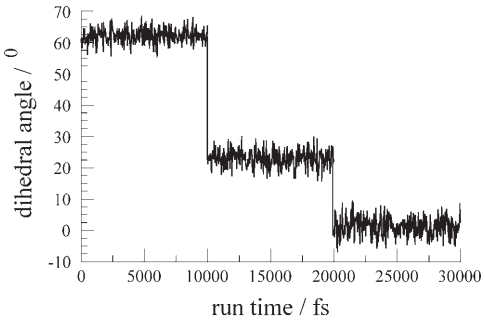

Figure 3. MDS run carried out for **C2**, each step corresponding to the addition of one electron.

ing ±5° of the mean value, but additional spikes were evident to show that more substantial distortions occurred with relatively low frequency. Addition of one electron, thereby forming the monocation radical, caused a marked decrease in the mean dihedral angle and increased the degree of thermal fluctuation (Figure 3). The standard deviation increased to around ±15° about the mean value, with occasional spikes in the geometries sampled. The mean φ value for the neutral species was close to 0°, as expected from the studies described above, but with a further increase in the fluctuation (Figure 3). The standard deviation was expanded to almost ±20° so that a wide variety of dihedral angles is sampled during the MDS run. Although it remains clear that there is a stepwise decrease in the mean φ value upon reduction of the viologen unit, the MDS runs indicate it is naive to expect any species to maintain a precise geometry in solution that can be compared with the electronic properties. Each of the samples behaved in a similar fashion.

Electronic coupling in the parent viologen: There are indications in the literature that the one-electron reduction poten-

tials ($E_{(1)RED}$) of certain viologen salts are influenced by the molecular conformation. Thus, the so-called diquat series exhibits variable reduction potentials that depend on the strap length,[12] as illustrated in the Supporting Information. The corresponding 1,10-phenanthrolinium compounds show a similar tend,[12] although data are highly restricted. Quantum chemical calculations made for MV^{2+} indicate that the planar form is more stable than the orthogonal geometry by approximately 9 kJ mol^{-1}, whereas the same calculations made for the monocation radical suggest that the planar species is energetically more favorable than the orthogonal form by about 100 kJ mol^{-1}. This last finding can be explained in terms of the relative resonance energies associated with the radical. Both the LUMO energy (E_{LUMO}) of the dication and the heat of formation of the monocation radical are dependent on the central torsion angle (see Supporting Information), with an evident destabilization at 90°. These various properties can be used to argue that the electronic properties of the constrained viologens will likely depend on the central dihedral angle.

In exploring how changes in torsion angle affect the electronic properties of MV^{2+}, we can consider three experimental approaches; namely, cyclic voltammetry, UV-visible absorption spectroscopy, and EPR spectroscopy. For MV^{2+}, successive electron additions occur with reduction potentials of −0.35 and −0.76 V versus SCE in deoxygenated acetonitrile solution (Table 2). The difference between these values,

Table 2. Summary of the electrochemical properties recorded for the various viologens in deoxygenated acetonitrile at 20°C.

	$E_{(1)RED}$ [V vs. SCE]	ΔE_{P1} [mV]	$E_{(2)RED}$ [V vs. SCE]	ΔE_{P2} [mV]	ΔE_{RED} [mV]
MV^{2+}	−0.35	70	−0.76	70	410
C1	−0.31	51	−0.73	61	420
C2	−0.87	66	−1.15	67	280
C3	−0.64	58	−0.87	60	230
C4	−0.64	67	−0.91	67	270
C5	−0.68	58	−0.91	62	230

which gives access to the comproportionation constant,[33] provides an indirect measure of electron delocalization at the monocation radical stage. The absorption spectrum of the monocation radical in deoxygenated acetonitrile shows pronounced transitions cantered at 608 and 400 nm (see Supporting Information). Both sets of bands show fine structure that can be deconvoluted into series of Gaussian-shaped components with vibrational spacings of about 1440 and 700 cm^{-1}, respectively. The overall spectrum, however, shows the presence of several other sets of transitions in both the visible and near-UV regions. The EPR spectrum recorded for the moncation radical in deoxygenated acetonitrile shows a series of well-resolved lines (see Supporting Information).[34] This spectrum can be simulated[18] on the basis of complete electron delocalization around the bipyridinium nucleus, including the aza N atoms and the methyl groups.[35] This behavior is consistent with a high degree of resonance stabilization of the radical[36] and, in particular, confirms that the central C–C bond acquires some degree of double-bond character, with the radical moving towards a planar geometry.

Cyclic voltammetry for the constrained analogues: Each of the strapped viologens undergoes two well-defined, one-electron reduction processes in deoxygenated acetonitrile containing TBAB background electrolyte (Figure 4). Both

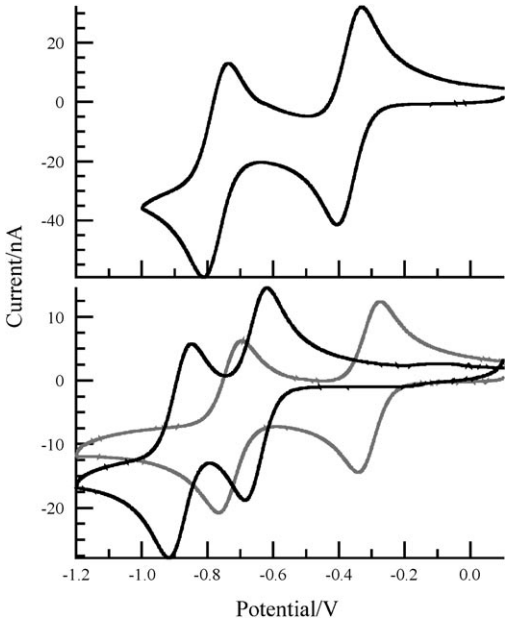

Figure 4. Typical cyclic voltammograms recorded for methyl viologen (upper panel), **C1** (lower panel; light curve), and **C2** (lower panel; dark curve) in deoxygenated acetonitrile containing background electrolyte.

processes are electrochemically reversible ($\Delta E_p \approx 60$ mV). The reduction potentials, calculated as the average between cathodic and anodic peaks, are listed in Table 2. In addition to considerable variation in the reduction potentials for addition of the first ($E_{(1)RED}$) and second ($E_{(2)RED}$) electrons, there is surprising lack of consistency in the difference between these values (ΔE_{RED}). By comparison to MV^{2+}, the two reductive steps are assigned to formation of the π-radical cation and the neutral species, respectively. The magnitude of the measured reduction potentials does not vary progressively with the length of the tether, but for the first reduction step there is a crude correlation with the central dihedral angle calculated for the dication. This behavior is in agreement with that found for the diquat series,[12] in which the first reduction potential moves towards more negative values as the dihedral angle increases (see Supporting Information), and with the effect of φ on the computed LUMO energy of MV^{2+}. In this way, the large disparity in first reduction potentials measured for **C1** and **C2** can be attributed to changes in molecular geometry. The effect can be traced to the fact that the energy of the LUMO depends on the molecular orientation and, in particular, on the

degree of planarity. This behavior is carried through to the second reduction step for which $E_{(2)RED}$ shows a crude dependence on the computed geometry of the monocation radical.

Apart from **C1**, the potential difference between addition of the first and second electrons is fairly constant at around 250 mV, but this is much less than the ΔE_{RED} value found for the parent viologen. In contrast, **C1** exhibits a similar ΔE_{RED} value to that of the parent. This situation can be explained in terms of the relative degrees of electron delocalization at the π-radical cation stage. Thus, both MV^{2+} and **C1** form monocation radicals that adopt structures in which the two aromatic rings are close to being parallel; this favors electron delocalization around the bipyridinium unit. Consequently, addition of the second electron is hindered with respect to the first reduction step, because of the raised electron density. The other strapped derivatives form distorted radical cations in which the two rings are held at dihedral angles of around 20°. This geometry is less favorable for extended π-electron delocalization, with the net result that attachment of the second electron becomes easier. This has the overall effect of ensuring that the actual reduction potentials are set by the dihedral angle of the dication.

Spectroelectrochemistry: The parent viologen exhibits a well-defined absorption band in the UV region, with a maximum (λ_{max}) at 255 nm and with a molar absorption coefficient (ε_{max}) of 17400 $M^{-1}\,cm^{-1}$ at the peak maximum in acetonitrile. This absorption band corresponds to the HOMO–LUMO transition. The strapped viologens show a similar absorption process, but, in each case, the accidental degeneracy is lost because of symmetry breaking by the tether, and two closely-spaced transitions are seen (Table 3). In the case of the most distorted viologen, namely **C2**, it is possible to resolve three transitions in the UV region. For each viologen, the lowest energy absorption transition has a ε_{max} of around 11000 $M^{-1}\,cm^{-1}$, while that of the higher energy transition is somewhat smaller. Controlled potential reduction of MV^{2+} in deoxygenated acetonitrile gives rise to the known blue coloration characteristic of the radical cation. The absorption spectrum of this radical comprises a series of two-overlapping transitions in the region from 500 to 800 nm and a set of sharper bands centered at around 400 nm that can be assigned to a single transition (see Supporting Information). The absorption bands evident in the visible region, having a ε_{max} of 10970 $M^{-1}\,cm^{-1}$ at 608 nm, are spin allowed and involve transitions from the two highest energy HOMO's to the SOMO. The higher energy band, located at 400 nm (ε_{max} = 35460 $M^{-1}\,cm^{-1}$) is assigned to the transition from the SOMO to the LUMO. On reduction to the neutral species, the lower energy transitions disappear, but the strong near-UV transition persists, albeit somewhat broadened, and slightly shifted to 398 nm (ε_{max} = 35270 $M^{-1}\,cm^{-1}$). This latter transition is from what was the SOMO but is now filled to the LUMO.

Table 3. Summary of the optical absorption spectral properties recorded for the various viologens in deoxygenated acetonitrile at 20°C by using spectroelectrochemical techniques.

	dication		monocation		neutral	
	λ_{max}[a]	ε_{max}[b]	λ_{max}[a]	ε_{max}[b]	λ_{max}[a]	ε_{max}[b]
C1	279	13720	428	26925	414	33120
	330	10460	652	10860		
			721	10580		
C2	244	15800	428	11880	413	28620
	288	10910	750	11500		
	330	4490				
C3	254	10500	417	10320	412	27390
	301	11580	790	7345		
C4	260	8850	427	11190	415	28500
	313	12500	800	9250		
C5	244	6250	435	12425	419	26930
	288	11680	715	9110		

[a] Peak maximum in nm. [b] Molar absorption coefficient in $M^{-1}\,cm^{-1}$.

The absorption spectrum recorded for the radical cation derived from **C1** bears some resemblance to that described for $MV^{\bullet+}$ and, in particular, both visible and near-UV transitions are clearly observed (Figure 5). The higher energy band, which is attributed to the SOMO–LUMO transition, is broadened with respect to that of the parent and shifted from 400 to 415 nm. There is a modest decrease in ε_{max} (Table 3). Again, deconvolution of this absorption band into Gaussian components indicates that only a single transition is involved. The lower energy transition, which involves two overlapping bands due to HOMO–SOMO transitions as in the case of $MV^{\bullet+}$, shows two clear maxima at 652 and 721 nm, both displaying similar ε_{max} values to that of $MV^{\bullet+}$. On reduction to the neutral species, a single transition is observed with a maximum at 414 nm and a relatively high ε_{max} (Table 3). As for MV, this band corresponds to a single transition and is somewhat broadened relative to the HOMO–LUMO transition associated with the corresponding dication.

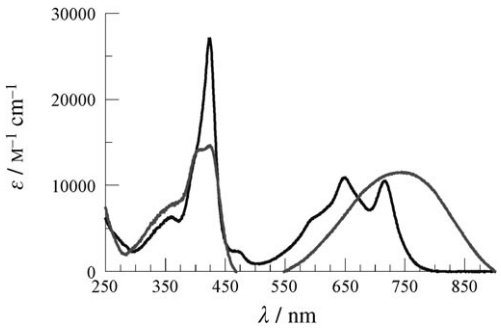

Figure 5. Examples of the absorption spectra of the monocation radicals derived for **C1** (dark curve) and **C2** (light curve) using spectroelectrochemical techniques in deoxygenated acetonitrile.

Viologen **C2**, which has the most distorted ground-state geometry and is more difficult to reduce than the other species, shows somewhat similar spectral characteristics for the reduced species, but it is noticeable that the lower energy

transition seen for the radical cation has lost all vibronic fine structure (Figure 5). This band has a maximum at 750 nm, but spectral deconvolution indicates that there are two overlapping transitions. The derived ε_{max} remains similar to that found for $MV^{\bullet+}$ (Table 3). The higher energy transition appears as two bands of comparable intensity and has a maximum at about 428 nm. As expected, the HOMO–SOMO transitions disappear on further reduction but the HOMO–LUMO transition is seen clearly with a maximum at 413 nm. For **C3**, the monocation radical displays a remarkably similar absorption spectrum to that described for **C2**, with the two bands being centered at 790 and 417 nm (Table 3). Again, the HOMO–SOMO transition shows no fine structure. In this case, the neutral species has the HOMO–LUMO transition located at 412 nm, but with a well-resolved shoulder on the low-energy side. The absorption spectral properties found for **C5** remain remarkably similar, with the SOMO–LUMO transition being centered at 435 nm and displaying vibronic structure. The HOMO–SOMO transitions are slightly split and clearly evident in the 600–800 nm range (Table 3). Here, the neutral species shows a pronounced HOMO–LUMO transition at 419 nm with a well-resolved shoulder (Table 3). The reduced forms of these three viologens exhibit quite similar absorption spectra, with some minor unique features, that differ from those of both **C1** and the parent viologen. Such behavior seems consistent with their somewhat comparable structural facets.

Viologen **C4** is the least soluble member of this series and the solubility is further decreased on reduction. For the monocation radical derived from **C4**, the SOMO–LUMO transition is relatively broad and centered at around 427 nm with a pronounced shoulder on the low-energy side. In fact, the shoulder is very evident for this species. Given the restricted solubility of this compound, it is likely that reduction is accompanied by self-association of the radical cation under the conditions used for the spectroelectrochemical studies. This raises the possibility that the low-energy shoulder is due to a dimer or a conjugate formed by association between a π-radical cation and a dication. Indeed, on repeating the experiments at much lower concentration, leading to a concomitant loss in signal-to-noise ratio, the shoulder disappears but the other spectral features remain. The HOMO–SOMO absorption bands appear as a single, broad transition centered at 800 nm (Table 3). The neutral species displays the broad HOMO–LUMO transition centered at 410 nm, with a ε_{max} value comparable to the other compounds.

In summary, the absorption spectra of the strapped viologens are characterized by a split HOMO–LUMO transition centered in the UV region. The lowest energy transition has a ε_{max} of about $11\,000\,M^{-1}\,cm^{-1}$, while that of the higher energy transition is approximately $8000\,M^{-1}\,cm^{-1}$ (Table 3). The combined oscillator strength is comparable to that of MV^{2+}, in which the two transitions are accidentally degenerate. A somewhat similar situation has been reported previously for certain tethered quaterphenyl derivatives.[30] The corresponding neutral species show a single transition at slightly lower energy, for which the average ε_{max} is on the order of $30\,000\,M^{-1}\,cm^{-1}$. There are only slight variations in the HOMO–LUMO gaps for these species, as might be expected from the observation that the computational studies predict geometries that are essentially planar. The radical cations display two sets of transitions: The highest energy band is centered at around 420 nm and is due to a single transition. There is a wide variation in ε_{max} for this band that cannot be explained in terms of partial self-association, although this is evident for **C4**, while vibronic structure is observed only for MV^{2+} and **C1**. We have assigned this band to a transition from the SOMO to the LUMO and the comparable energy gaps arise, because the energies of these two orbitals show similar dependence on the dihedral angle. Vibrational fine structure is observed only for planar geometries, for which the transition is relatively intense. Raising the potential energy of the SOMO, by increasing the dihedral angle, serves to eliminate the vibronic fine structure and decrease the absorption coefficient.

The radical cations also absorb at lower energy and here there is a good level of consistency in the ε_{max} values (Table 3). Spectral deconvolution indicates the presence of two overlapping transitions in each case, but both the spectral profiles and the band maxima change with the nature of the compound. Again, vibronic fine structure is observed only when the structures are close to being planar. Both absorption bands are assigned to HOMO–SOMO transitions, but the respective energy gaps vary quite noticeably among the compounds. In fact, the HOMO–SOMO energy gaps decrease steadily with increasing potential energy of the HOMO, as imposed by the dihedral angle. This situation requires that the energy of the SOMO depends less critically on changes in this angle.

EPR spectroscopy: Several prior studies[34,35] have addressed the EPR properties of the moncation radical derived from the parent viologen $MV^{\bullet+}$ and from viologens bearing different substituents at the aza N atoms.[37] In our work, $MV^{\bullet+}$ was generated by in situ electrochemical reduction in deoxygenated acetonitrile and the EPR spectrum was recorded at room temperature (see Supporting Information), for which the *g* factor was found to be 2.0031. The spectrum could be simulated[18] on the basis of the radical centre coupling to two equivalent N atoms, with a hyperfine coupling constant (a_N) of 0.423 mT, and 14 H atoms. The latter can be divided into protons on the methyl groups ($a_{Me} = 0.399$ mT) and two equivalent sets, each of four protons, on the aromatic nucleus. On the basis of earlier work[34,35] and INDO calculations,[37] the hyperfine coupling constants for these aryl H atoms can be assigned to the C^{α} ($a_{CH} = -0.133$ mT) and C^{β} ($a_{CH} = -0.157$ mT) sites. Calculations made at the INDO level have indicated[26d] that the central torsion angle has a modest effect on the a_{CH} values once φ exceeds about 15°. In particular, these calculations predict a decrease in a_{CH} for both the methyl protons and those located at C^{α}, but an increase in a_{CH} for the C^{β} protons. In turn, this suggests that

the strapped viologens might display unique EPR spectral properties characteristic of the dihedral angle, although it is realized that the presence of the strap will complicate the spectrum.

EPR spectra were recorded for the radical cations derived from each of the strapped viologens in deoxygenated acetonitrile (Figure 6), and the spectral patterns were

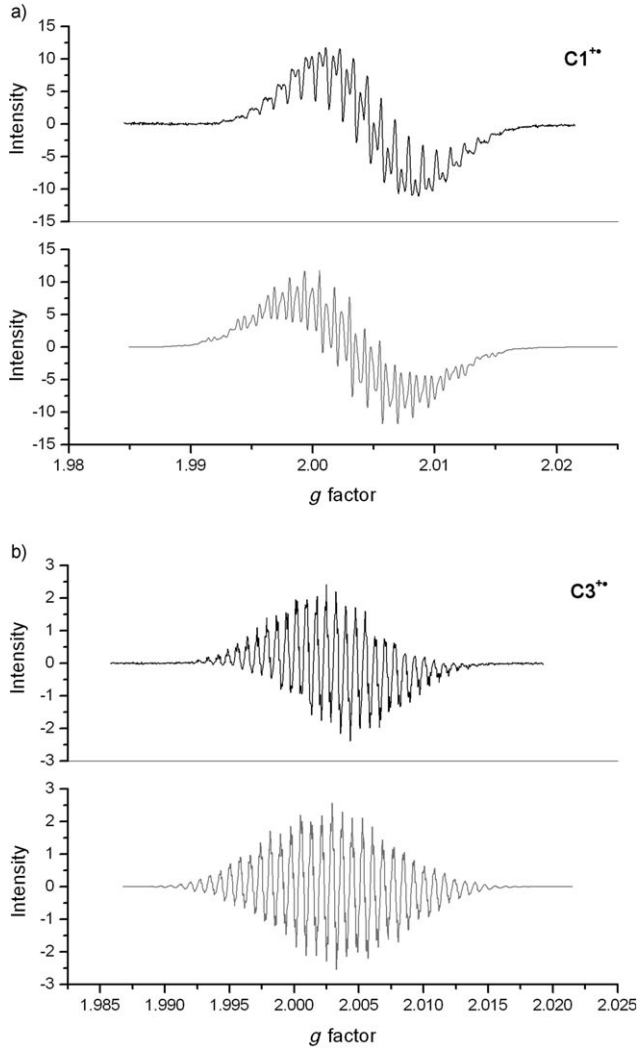

Figure 6. Examples of the EPR spectra (dark) and simulated spectra (grey) recorded for the monocation radicals derived for **C1** (upper panel) and **C3** (lower panel) in deoxygenated acetonitrile at room temperature.

subsequently simulated as above. In each case, the g factor was found to be close to 2.0030 and the fitting parameters are summarized in Table 4. For the strapped viologens, three separate aromatic CH residues, each corresponding to two protons, can be distinguished and the participation of the tether has to be taken into account. Consequently, it is difficult to assign peaks to particular sets of CH sites, although the effects of the methyl groups and N aza atoms are easily resolved by comparison to the parent. The central dihedral

Table 4. Summary of the EPR spectral properties recorded for the various viologen radical cations in deoxygenated acetonitrile.[a]

	MV^{2+}	**C1**	**C2**	**C3**	**C4**	**C5**
g[b]	2.0031	2.0031	2.0030	2.0030	2.0031	2.0029
φ [°][c]	1.3	10.1	22.8	25.8	21.3	21.1
a_{Me}	0.399	0.428	0.405	0.400	0.418	0.416
a_N	0.423	0.433	0.424	0.414	0.430	0.427
C^{α}[d]	−0.157	−0.213	−0.263	−0.285	−0.251	−0.256
C^{β}[d]	−0.133	−0.189	−0.127	−0.112	−0.135	−0.129
C^{χ}[d]	−0.157	−0.097	−0.114	−0.135	−0.119	−0.115
a_S	–	−0.063	−0.014	0.017	−0.037	−0.038

[a] All hyperfine coupling constants are given in units of mT. [b] g factor. [c] Central dihedral angle for the monocation radical. [d] a_{CH} value.

angle affects both a_N and a_{Me} (Table 4). Thus, there is a small (i.e., about 5%) decrease in the hyperfine coupling constant for both sites as the central dihedral angle increases from 10° to 26° and this behavior seems to be fully consistent with the INDO calculations reported[26d] earlier for $MV^{\bullet+}$. A similar effect is observed for coupling with carbon atoms on the tether, these also being readily identifiable, although the actual values are small because of the distance and insulating properties of the bridging O atoms.

Hyperfine coupling constants for the CH sites on the aromatic rings were identified on the basis of INDO calculations (Table 4). Although these values differ markedly from those recorded for the parent (in which $C^{\alpha}=C^{\chi}$), comparison is difficult because of the contributory effects of induction by the alkoxy substituent and the change in φ. It can be seen that a_{CH} for the C^{α} position, taken as the modulus, increases quite significantly with increasing φ. The same behavior is found for the C^{χ} site, but a_{CH} for the C^{β} position decreases steadily with increasing dihedral angle. Consequently, the main effect of increasing the dihedral angle is to modify the distribution of the spin density around the ring. The C^1 and N positions are not much affected, nor are sites on the strap (a_S), so that the predominant changes occur at the ring. Because the monocation radical attempts to reach a planar geometry, despite the presence of the strap, it has been possible to achieve only a modest variation in φ, but nonetheless these experimental findings are in qualitative agreement with prior INDO calculations carried out for the parent viologen.[26d] A common practice in EPR spectroscopy[38] is to examine the effects of changing φ on individual a_{CH} values by way of expressions such as that given as Equation (1). Here, ζ_0 refers to an inherent (i.e., angle-independent) hyperfine coupling constant and ζ_{90} is an angle-dependent hyperfine coupling constant for which the modulus is at a maximum when the two rings lie coplanar.

$$a_{CH} = \zeta_0 + \zeta_{90}\cos^2\phi \quad (1)$$

The limited variation in φ hinders accurate correlation of the observed a_{CH} values with dihedral angle, although there is a good fit to Equation (1) for each of the aryl CH sites. This crude observation allows us to separate the inductive effect from the angle dependence and thereby to assign spin

densities to the individual sites. Thus, extrapolation of the data to $\varphi = 0°$ gives individual a_{CH} values that can be compared directly with those observed for the parent viologen under identical conditions and in which the rings are essentially coplanar (Table 5). The difference between these two

Table 5. Comparison of the hyperfine coupling constants and spin densities derived for the strapped and parent viologen radical cations at coplanar and orthogonal geometries.[a]

a_{CH} [mT]	parent	strapped
ζ_0/C^{α}	−0.157 (0.052)	−0.197 (0.066)
ζ_0/C^{β}	−0.133 (0.044)	−0.201 (0.067)
ζ_0/C^{χ}	−0.157 (0.052)	−0.089 (0.030)
ζ_{90}/C^{α}	−0.166 (0.055)	−0.640 (0.213)
ζ_{90}/C^{β}	+0.008 (0.003)	+0.296 (0.099)
ζ_{90}/C^{χ}	−0.166 (0.055)	−0.306 (0.102)

[a] The modulus of the computed spin density is given in parenthesis after the hyperfine coupling constant.

sets of data can be attributed to the inductive effect of the alkoxy group, since the geometry is now fixed. Furthermore, on the basis of the McConnell equation[39] [Eq. (2)], for which earlier work[40] has established that the constant Q has value of 3.0 mT for the aryl CH sites of MV^{2+}, it becomes possible to estimate values for the spin density (ρ) at that carbon atom (Table 5). Comparing these data shows that the alkoxy group has only a modest effect on the spin density at the C^{α} position. More significant effects are observed, however, at the other two aryl CH sites at which it appears that the inductive effect serves to transfer spin density from C^{χ} to C^{β}. The net effect is that whereas the spin density is evenly distributed around the CH positions in the parent radical ,there is a tendency to localize spin density at the C^{α} and C^{β} sites while depleting that at the C^{χ} position.

$$a_{CH} = \rho Q \qquad (2)$$

Now, the effects of twisting around the interring bond can be seen for the strapped viologens by extrapolation to $\varphi = 90°$. The main conclusion is that the spin density for both C^{α} and C^{χ} sites increases quite dramatically as φ approaches 90°, with the effect on C^{α} being particularly noticeable (Table 5). This situation arises because these a_{CH} values increase with increasing dihedral angle. In contrast, the spin density at the C^{β} position increases less significantly with increasing φ and there is a change in sign for the orthogonal geometry. For this position, the a_{CH} increases with increasing dihedral angle. Quite similar behavior has been computed for the parent system, in which rotation around the connecting bond is predicted to have little effect on the spin density at the C^{α} site. As found for the strapped analogues, however, moving to the orthogonal geometry is expected to essentially remove the spin density from the C^{β} position, and again this is accompanied by a change in sign (Table 5). Therefore, the strap does not perturb the electronic properties of the viologen, but it serves to redistribute the spin density via an inductive effect.

Conclusion

The approach taken here is a viable strategy for the systematic variation of the central dihedral angle of poly(aryl) systems. It works particularly well for the ground-state molecules, although there is some bending of the isolated species as a means by which to relieve the applied stress,[30] but is less successful for cases in which resonance stabilization is important. In fact, the radical cations react against the strap in an attempt to attain coplanar geometries having increased bond order for the inter-ring C–C bond. This effect is emphasized for the neutral species where the ideal geometry is based on a connecting C=C bond. Nonetheless, the length of the tether does have a significant effect on the electronic properties of the molecule. It should be noted that this is the first class of tethered molecules for which we have been able to relate the electronic properties to changes in the interring dihedral angle. This is because of the facile reduction to a stable moncation radical; in other cases attention has been restricted to the photophysical properties[13b] or to indirect electronic properties like the rates of through-bond electron exchange.[13a,15] With this viologen series,[16] it has been possible to assess how alterations in the dihedral angle influence the distribution of spin density around the aryl ring and help set the magnitude of the reduction potentials. The key feature with these compounds is that the energy of the LUMO depends critically on the dihedral angle.

On-going research is set to explore the possibility of using more rigid tethers that will prevent the reduced species from minimizing the dihedral angle and in developing analogues where the conformation can be switched rapidly by external stimulation. These materials will form the basis of artificial neural networks intended to direct electron flow along predetermined routes by modulating the redox properties of interspersed viologen relays. On the basis of the calculated LUMO energies, it can be expected that the reduction potential could be varied over a range of about 0.9 V on switching the geometry from planar to orthogonal. This is more than enough to control the rate of electron transfer and it is now realized that large changes in spin density, and presumably other factors such as charge density, can be achieved by conformational exchange of the type described here. As such, the idea of directing electrons along certain pathways of a network by gating the orientation of particular subunits looks to be very attractive.

Experimental Section

All chemicals were purchased from Aldrich Chemical Co. and were used as received. The starting materials diethylcarbamic acid pyridin-3-yl ester (**2**), diethylcarbamic acid 4-iodopyridin-3-ol (**3**), and 4-iodopyridin-3-ol (**4**) were prepared by literature methods.[16] Solvents were dried by standard literature procedures before being distilled and stored under nitrogen over 4 Å molecular sieves.[17] ^1H and ^{13}C NMR spectra were recorded with a JEOL Lambda 500 MHz or Bruker AVANCE 300 MHz spectrometer. Routine mass spectra and elemental analyses were obtained using

in-house facilities. Spectroscopic grade solvents were obtained from Aldrich Chemical Co. and were redistilled before use.

Preparation of 3-diethylcarbamic acid (pyridin-4-yl boronic acid) ester (5): $B(OiPr)_3$ (3.2 mL, 13.6 mmol) was added to a solution of **2** (2.00 g, 10.3 mmol) in THF (30 mL) under an N_2 atmosphere. The solution was cooled to −78 °C and *t*BuLi (7.5 mL, 1.7 M in pentane) was added by syringe pump over a period of 1 h. The light yellow mixture was held at −78 °C for 1 h. The dry ice/acetone bath was removed and the mixture was allowed to warm to −20 °C. Then 2 M HCl (10 mL) was added and the mixture stirred until reaching RT. To this solution was added a mixture of toluene (50 mL) and 2 M HCl (10 mL). The aqueous layer was separated, and the organic layer washed with 2 M HCl. The combined aqueous layers were neutralized with 5 M NaOH, to afford a white precipitate. The suspension was extracted with EtOAc, dried over $MgSO_4$, filtered, and evaporated on a rotary evaporator. The residual white solid was washed with diethyl ether and used without further purification in the following reaction (1.6 g, 65 % yield). ^{1}H NMR (300 MHz, CD_3OD): $\delta = 1.29$ (m, 6H; H of -CH_3), 3.46–3.64 (m, 4H; H of -NCH_2-), 7.50 (d, $J = 4.7$ Hz, 1H; Py-H^5), 8.37 ppm (m, 2H; Py-$H^{2,6}$); ^{11}B NMR (CD_3OD): $\delta = 19.3$ ppm.

Preparation of diethylcarbamic acid 3′-hydroxy-4,4′-bipyridin-3-yl ester (6)

Method I: $[Pd(PPh_3)_4]$ (0.22 g, 0.19 mmol) was added to an N_2-purged solution of **3** (1.0 g, 3.1 mmol) in DME (40 mL). The light yellow solution was stirred at RT for 10 min. Compound **5** (1.1 g, 4.6 mmol) in deoxygenated ethanol (10 mL) and 1 M Na_2CO_3 (9.4 mL) was added to this solution. The mixture was refluxed overnight after which time TLC showed complete consumption of **3**. Water (50 mL) and EtOAc (100 mL) were poured into the solution, which was filtered to remove insoluble material. The isolated organic layer was washed with 0.2 M Na_2CO_3 (2×100 mL). The combined aqueous layers were washed with EtOAc (30 mL) and neutralized with 2 M HCl. The cloudy suspension which formed was extracted with EtOAc, dried over $MgSO_4$, and filtered. Removal of the organic solvents afforded an oily solid (0.76 g, 85 % yield). ^{1}H NMR (300 MHz, CD_3OD): $\delta = 1.04$ (m, 6H; H of -N-CH_2-), 3.29 (m, 4H; H of -CH_3), 7.28 (d, $J = 4.9$ Hz, 1H; H of Py), 7.51 (d, $J = 4.9$ Hz, 1H; H of Py), 8.18 (m, 2H; H of Py), 8.52 ppm (m, 2H; H of Py).

Method II: $B(OiPr)_3$ (3.2 mL, 13.6 mmol) was added to a solution of **2** (2.00 g, 10.3 mol) in THF (25 mL). The solution was cooled to −78 °C and *n*BuLi (8.0 mL, 1.6 M in hexane) was added by syringe pump over a period of 1 h. The yellow mixture was held at −78 °C for 1 h. The dry ice/acetone bath was removed and the mixture was allowed to warm to RT and stirred for a further 1 h. Deoxygenated ethanol (10 mL) was added to the solution. The mixture was transferred to a pre-mixed solution of **3** (1.5 g, 4.7 mmol) and $[Pd(PPh_3)_4]$ (0.34 g, 0.29 mmol) in DME (45 mL), followed by the addition of deoxygenated ethanol (20 mL) and 1 M Na_2CO_3 (14 mL). The mixture was refluxed overnight and TLC confirmed completion of the reaction. Workup as described in Method I afforded an oily solid. Yield: 1.15 g (84 %, based on starting material **3**).

Preparation of 4,4′-bipyridinyl-3,3′-diol (7): 2 M NaOH (32 mL) was added to a solution of **6** (4.54 g, 16.0 mmol) in methanol (40 mL). The mixture was refluxed overnight, cooled to RT and filtered. The filtrate was reduced in volume to about 5 mL, and water was added to the residue before being filtered. The yellow filtrate was acidified to pH ~ 5 with 6 M HCl, to afford a yellow precipitate. Yield 2.23 g, 75 %; ^{1}H NMR (300 MHz, $[D_6]$DMSO): $\delta = 7.44$ (d, $J = 4.9$ Hz, 2H; Py-H^6), 8.15 (d, $J = 4.9$ Hz, 2H; Py-H^5), 8.32 (s, 2H; Py-H^3), ≈11 ppm (br s, 2H; -OH); EI-MS: *m*/*z* calcd for $C_{10}H_8N_2O_2$: 188.06; found: 188.

Preparation of 1,2-bis(4-iodo-pyridin-3-yl)propane (8): *t*BuOK (1.22 g, 10.9 mmol) was added to a solution of **4** (2.0 g, 9.1 mmol) in DMF (30 mL)/THF (10 mL) held under an N_2 atmosphere at −15 °C; the resulting mixture was stirred at −15 °C for 30 min. 1,3-Bis(toluene-4-sulfonyloxy)propane (1.60 g, 4.16 mmol) in DMF (15 mL)/THF (5 mL) was added over one hour at −15 °C. The mixture was stirred at RT overnight. The resultant brown suspension was isolated and extracted with EtOAc. The EtOAc layer was washed with aqueous Na_2CO_3, separated, and dried over $MgSO_4$. The resultant crude product obtained after solvent removal was purified by silica-gel chromatography with petrol/ethyl acetate (1:20) as the eluant to produce a pale yellow solid (1.20 g, 60 % yield). ^{1}H NMR (δ, 300 MHz, $[D_8]$THF): $\delta = 2.53$ (quint, $J = 6.0$ Hz, 2H; H of -CH_2-), 4.60 (t, $J = 6.0$ Hz, 4H; H of -OCH_2-), 7.87 (d, $J = 4.9$ Hz, 2H; Py-H^5), 7.97 (d, $J = 4.9$ Hz, 2H; Py-H^6), 8.38 ppm (s, 2H; Py-H^2); EI-MS: *m*/*z* calcd for $C_{13}H_{12}I_2N_2O_2$: 481.9; found: 482.

General procedure for the synthesis of 1a–1e: NaH (1.1 equiv) was added to a solution of **7** (400 mg, 2.10 mmol) in DMF (60 mL) under an N_2 atmosphere. The mixture was stirred at RT for 1 h. The ditosyloxy linker (1.2 equiv) or CH_2I_2 (1.2 equiv) in DMF (20 mL) was added slowly through a syringe pump to this solution. The mixture was stirred at RT for ≈24 h and the DMF was removed under reduced pressure. The resultant residue was extracted with EtOAc, washed with H_2O, and dried over $MgSO_4$. Removal of the solvent afforded the crude product, which was purified by column chromatography.

*Data for **1a***: Compound **7** (0.40 g, 2.10 mmol), CH_2I_2 (0.25 mL, 3.1 mmol); silica gel, petrol/acetone (2:3); yield: 40 mg, 9 %, off-white solid; ^{1}H NMR (300 MHz, CD_2Cl_2): $\delta = 5.55$ (s, 2H; H of methylene), 7.78 (d, $J = 5.4$ Hz, 2H; Py-H^6), 8.39 (d, $J = 5.4$ Hz, 2H; Py-H^5), 8.48 ppm (s, 2H; Py-H^3); EI-MS: *m*/*z* calcd for $C_{11}H_8N_2O_2$: 200.06; found: 200.

*Data for **1b***: Compound **7** (0.40 g, 2.10 mmol), 1,2-bis(toluene-4-sulfonyloxy)-ethane (0.94 g, 2.50 mmol); silica gel, petrol/acetone (1:2); yield: 58 mg, 13 %, off-white solid; ^{1}H NMR (300 MHz, CD_2Cl_2): $\delta = 4.29$ (br s,4H; H of ethylene), 7.26 (d, $J = 4.9$ Hz, 2H; Py-H^6), 8.44 (d, $J = 4.9$ Hz, 2H; Py-H^5), 8.47 ppm (s, 2H; Py-H^3); EI-MS: *m*/*z* calcd for $C_{12}H_{10}N_2O_2$: 214.07; found: 214.

*Data for **1c***: Compound **7** (0.40 g, 2.10 mmol), 1,3-bis(toluene-4-sulfonyloxy)propane (0.98 g, 2.50 mmol; silica gel, petrol/acetone (1:3); yield: 89 mg, 18 %, off-white solid; ^{1}H NMR (300 MHz, CD_2Cl_2): $\delta = 2.05$ (quint, $J = 5.2$ Hz, 2H; H of -CH_2-), 4.42 (t, $J = 5.2$ Hz, 4H; H of -OCH_2-), 7.18 (d, $J = 4.7$ Hz, 2H; Py-H^6), 8.36 (d, $J = 4.7$ Hz, 2H; Py-H^5), 8.47 ppm (s, 2H; Py-H^3). EI-MS: *m*/*z* calcd for $C_{13}H_{12}N_2O_2$: 228.09; found: 228. A minor byproduct **1f** resulting from the elimination of the tosylate was isolated in varying yield, depending on the nature and quantity of the base applied. ^{1}H NMR (300 MHz, CD_2Cl_2): $\delta = 4.60$ (m, 4H; H of =CH_2), 5.21 (m, 4H; H of -OCH_2-), 5.92 (m, 2H; H of -CH=), 7.20 (d, $J = 4.6$ Hz, 2H; Py-H^6), 8.26 (d, $J = 4.6$ Hz, 2H; Py-H^5), 8.33 ppm (s, 2H; Py-H^3); EI-MS: *m*/*z* calcd for $C_{16}H_{16}N_2O_2$: 268.3; found: 268.

*Data for **1d***: Compound **7** (0.40 g, 2.1 mmol), 1,4-bis(toluene-4-sulfonyloxy)butane (1.02 g, 2.6 mmol); silica gel, petrol/acetone (1:5); yield: 168 mg, 33 %, off-white solid; ^{1}H NMR (300 MHz, CD_2Cl_2): $\delta = 1.91$ (br s, 4H; H of -CH_2CH_2-), 4.20 (br s, 2H; H of -OCH_2-), 4.62 (br s, 2H; H of -OCH_2-), 7.21 (d, $J = 4.8$ Hz, 2H; Py-H^6), 8.29 (d, $J = 4.8$ Hz, 2H; Py-H^5), 8.42 ppm (s, 2H; Py-H^3); EI-MS: *m*/*z* calcd for $C_{14}H_{14}N_2O_2$: 242.1; found: 242.

*Data for **1e***: Compound **7** (0.40 g, 2.10 mmol), bis-{2-[2-(toluene-4-sulfonyoxy)-ethoxy]ethyl}ether (1.29 g, 2.60 mmol); silica, petrol/acetone (1:20); yield: 140 mg, 19 %, oily solid; ^{1}H NMR (300 MHz, CD_2Cl_2): $\delta =$ 3.53 (m, 8H; H of -OCH_2-), 3.74 (m, 4H; H of -OCH_2-), 4.07 (m, 2H; H of -OCH_2-), 4.30 (m, 2H; H of -OCH_2-), 7.10 (d, $J = 4.7$ Hz, 2H; Py-H^6), 8.25 (d, $J = 4.7$ Hz, 2H; Py-H^5), 8.37 ppm (s, 2H; Py-H^3); EI-MS: *m*/*z* calcd for $C_{18}H_{22}N_2O_5$: 346.1; found: 346.

General procedure for the synthesis of C1–C5: CH_3I (5 equiv) was added to a solution of **1a** - **1e** (0.19–0.66 mmol) in CH_3CN (30 mL). The mixture was refluxed overnight; it was then cooled to RT and diethyl ether added to complete precipitation of the product. The resultant yellow to yellow-orange solid was filtered and washed thoroughly with diethyl ether. After drying, the solid was dissolved in water (ca. 30 mL) and aqueous KPF_6 solution (8 equiv) was added to precipitate the product. The pure product was obtained by recrystallization from acetonitrile and diethyl ether.

*Data for **C1***: Compound **1a** (38 mg, 0.19 mmol), CH_3I (0.20 mL, 3.20 mmol); yield: 57 mg, 57 %, pale yellow solid; ^{1}H NMR (300 MHz, CD_3CN): $\delta = 4.39$ (s, 6H; CH_3), 5.84 (s, 2H; H of methylene), 8.59 (br s, 4H; H of Py), 8.78 ppm (br s, 2H; H of Py); ^{13}C NMR (CD_3CN): $\delta = 48.0$, 96.3, 127.3, 134.4, 139.2, 140.2, 156.1 ppm; ES-MS: *m*/*z* calcd for $[M-2PF_6]^+$: 230.3; found: 231.0; *m*/*z* calcd for $[M-2PF_6]^{2+}$: 115.1;

found: 114.9; elemental analysis calcd (%) for $C_{13}H_{14}N_2O_2{\cdot}P_2F_{12}$: C 30.01, H 2.71, N 5.39; found: C 30.13, H 2.75, N 5.41.

Data for ***C2***: Compound **1b** (40 mg, 0.19 mmol), CH_3I (0.20 mL, 3.20 mmol); yield: 60 mg, 61%, pale yellow solid; ^{1}H NMR (300 MHz, CD_3CN): $\delta=4.39$ (s, 6H; CH_3), 4.73 (br s, 4H; H of ethylene), 8.09 (d, $J=6.2$ Hz, 2H; Py-H^6), 8.62 (d, $J=6.2$ Hz, 2H; Py-H^5), 8.75 ppm (s, 2H; Py-H^3); ^{13}C NMR (CD_3CN): $\delta=48.3$, 71.3, 128.7, 140.5, 140.8, 142.0, 155.2 ppm; ES-MS: m/z calcd for $[M-PF_6]^+$: 389.1; found: 389.1; m/z calcd for $[M-2PF_6-H]^+$: 243.3; found: 243.1; elemental analysis calcd (%) for $C_{14}H_{16}N_2O_2{\cdot}P_2F_{12}$: C 31.48, H 3.02, N 5.24; found: C 31.25, H 3.17, N 5.25.

Data for ***C3***: Compound **1c** (50 mg, 0.22 mmol), CH_3I (0.20 mL, 3.2 mmol); yield: 101 mg, 84%, pale yellow solid; ^{1}H NMR (300 MHz, CD_3CN): $\delta=2.25$ (q, $J=5.1$ Hz, 2H; H of -CH_2-), 4.39 (s, 6H; H of CH_3), 4.66 (t, $J=5.1$ Hz, 4H; H of -OCH2-), 8.04 (d, $J=6.1$ Hz, 2H; Py-H^6), 8.57 (d, $J=6.1$ Hz, 2H; Py-H^5), 8.77 ppm (s, 2H; Py-H^3); ^{13}C NMR (CD_3CN): $\delta=28.9$, 48.5, 74.3, 127.6, 137.4, 140.5, 141.6, 155.6 ppm; ES-MS: m/z calcd for $[M-PF_6]^+$: 403.1; found: 403.2; m/z calcd for $[M-2PF_6-H]^+$: 257.1; found: 257.1; m/z calcd for $[M-2PF_6]^{2+}$: 129.1; found: 128.9; elemental analysis calcd (%) for $C_{15}H_{18}N_2O_2{\cdot}P_2F_{12}$: C 32.86, H 3.31, N 5.11; found: C 33.15, H 3.49, N 5.10%.

Data for ***C4***: Compound **1d** (160 mg, 0.66 mmol), CH_3I (0.50 mL, 7.9 mmol).; yield: 270 mg, 73%, pale yellow solid; ^{1}H NMR (300 MHz, CD_3CN): $\delta=2.10$ (br s, 4H; H of -CH_2CH_2-), 4.32 (br s, 2H; H of -OCH_2-), 4.38 (s, 6H; CH_3), 4.80 (br s, 2H; H of -OCH_2-), 8.02 (d, $J=6.0$ Hz, 2H; Py-H^6), 8.48 (d, $J=6.0$ Hz, 2H; Py-H^5), 8.62 ppm (s, 2H; Py-H^3); ^{13}C NMR (CD_3CN): $\delta=27.3$, 48.4, 75.3, 128.3, 135.1, 138.1, 138.5, 155.5 ppm; ES-MS: m/z calcd for $[M-PF_6]^+$: 417.1; found: 417.1; m/z calcd for $[M-2PF_6-H]^+$: 271.3; found: 271.1; elemental analysis calcd (%) for $C_{16}H_{20}N_2O_2{\cdot}P_2F_{12}$: C 34.18, H 3.59, N 4.98; found: C 34.09, H 3.83, N 4.93.

Data for ***C5***: Compound **1e** (130 mg, 0.38 mmol), CH_3I (0.30 mL, 4.8 mmol); yield: 135 mg, 54%, pale yellow solid; ^{1}H NMR (300 MHz, CD_3CN): $\delta=3.49$ (m, 6H; H of -OCH_2-), 3.61 (m, 2H; H of -OCH_2-), 3.81 (m, 4H; H of -OCH_2-), 4.28 (m, 2H; H of -OCH_2-), 4.40 (s, 6H; CH_3), 4.49 (m, 2H; H of -OCH_2-), 7.91 (d, $J=6.0$ Hz, 2H; Py-H^6), 8.43 (d, $J=6.0$ Hz, 2H; Py-H^5), 8.63 ppm (s, 2H; Py-H^3); ^{13}C NMR (CD_3CN): $\delta=48.7$, 68.4, 69.8, 69.9, 70.7, 128.1, 131.7, 137.4, 137.5, 155.0 ppm; ES-MS: m/z calcd for $[M-PF_6]^+$: 521.2; found: 521.2; elemental analysis calcd (%) for $C_{20}H_{28}N_2O_5{\cdot}P_2F_{12}$: C 36.05, H 4.24, N 4.20; found: C 36.04, H 4.19, N 4.32%.

Absorption spectra were recorded in dilute acetonitrile on a Hitachi U3310 spectrophotometer. Cyclic voltammetric studies were carried out with a conventional three-electrode system controlled by an HCH Instruments Electrochemical Analyzer. The system used a glassy-carbon reference electrode, a platinum-wire counter electrode, and a silver/silver chloride reference electrode. Ferrocene was used as an internal standard in all voltammetric measurements. Solutions were prepared in acetonitrile containing approximately 1 mM analyte and 0.1 M tetra-*N*-butylammonium tetrafluoroborate (TBAB) as background electrolyte. The solution was purged thoroughly with nitrogen prior to the experiment and kept under a nitrogen atmosphere during measurements. Spectroelectrochemical studies were conducted in a Perkin–Elmer Lambda 35 spectrophotometer with the aid of an optically transparent thin-layer electrochemical cell (OTTEL) supplied by SpecAc. The OTTEL consisted of a platinum-mesh working electrode, a platinum-wire counter electrode, and a silver wire reference electrode and was controlled by the HCH Instruments Electrochemical Analyzer. Solutions were prepared in freshly distilled acetonitrile containing 1 mM analyte and 0.1 M TBAB as supporting electrolyte. Solutions were deoxygenated by purging with nitrogen for fifteen minutes prior to the experiment. Potentials were switched after electrolysis in order to confirm the full reversibility of the system.

Electron paramagnetic resonance (EPR) spectroscopic measurements were recorded on a Bruker X-band EPR spectrometer. The reduced viologens were generated in-situ by controlled potential electrolysis using a modified flat-cell with a platinum-mesh working electrode, a platinum-wire counter electrode and a silver/silver chloride reference electrode. Spectra were recorded in acetonitrile solution containing the analyte and 0.1 M TBAB. More than fifty scans were averaged for each compound in order to improve the signal to noise ratio. These measurements were made at the EPSRC-sponsored EPR Centre housed at the University of Manchester. The EPR data were simulated using XSophe, as part of the package supplied by Bruker.[18]

A summary of the crystallographic data for compounds **C1**–**C5** is given in Table S2. Data sets were collected on Nonius KappaCCD and Bruker SMART 1 K diffractometers with $Mo_{K\alpha}$ radiation ($\lambda=0.71073$ Å) for **C1**–**C4**. The small size and poor quality of crystals of **C5** necessitated the use of synchrotron radiation ($\lambda=0.6868$ Å) at Station 9.8 of the CCLRC Daresbury Laboratory SRS, with a Bruker APEX2 diffractometer. Programs were standard control and integration software (Bruker SMART, APEX2 and SAINT; Nonius COLLECT and EVALCCD), together with SADABS, SHELXTL and local programs. Disorder was resolved and successfully refined for a segment of the polyether strand of **C5**, the central CH_2 group of **C3**, and (extensively) the anions of **C1**. Hydrogen atoms were constrained with a riding model. The cations of **C1** and **C5** have no crystallographic symmetry. Compounds **C2**, **C3**, and **C4** were found to be isomorphous, with essentially the same basic structure differing only in the length of the linker strand; in each case a crystallographic twofold rotation axis passes through the centre of the strand and the centre of the C–C bond between the two pyridinium rings. CCDC–646986 (**C1**), CCDC-646987 (**C2**), CCDC-646988 (**C3**), CCDC-646989 (**C4**), and CCDC-646990 (**C5**) contain the supplementary crystallographic data for this paper. These data can be obtained free of charge from The Cambridge Crystallographic Data Centre via www.ccdc.cam.ac.uk/data_request/cif.

All quantum chemical calculations were made with the Gaussian 03 package.[19] For the ground-state molecules, calculations were made at the Hartree–Fock (HF) and Becke's three-parameter hybrid exchange functional with the Lee–Yang–Parr correlation functional (B3LYP) level and with the 6–31G(d,p) basis set. Solvent effects were examined using the polarized continuum model.[20] Spin-density calculations were made at the INDO level.[19] Classical dynamics of the viologens, starting from the energy-minimized geometries, were studied in a reservoir of 512 acetonitrile molecules by using CHARMM v.27b4 and with periodic boundary conditions.[21] In these simulations, the molecule under investigation was allowed to equilibrate for 2 ps before running the dynamics simulation over 10 ps, for each of the three oxidation states.

Acknowledgements

We thank the EPSRC (EP/C007727/1) and the University of Newcastle for financial support of this work. Electrospray mass spectra were recorded at the EPSRC-sponsored Mass Spectrometry Service at Swansea, and the EPR studies were made at the EPSRC-sponsored EPR Centre at the University of Manchester. We are especially grateful to Dr D. Collison for assistance and advice with these measurements. We also thank EPSRC and CCLRC for the use of the National Crystallography Service and access to synchrotron facilities at Daresbury Laboratory.

[1] P. M. S. Monk, *The Viologens: Physicochemical Properties, Synthesis and Applications of the Salts of 4,4′-Bipyridine*, Wiley, Chichester, **2001**.

[2] L. A. Summers, *The Bipyridinium Herbicides*, Academic Press, London, **1980**.

[3] a) J. R. Darwent, P. Douglas, A. Harriman, G. Porter, M. C. Richoux, *Coord. Chem. Rev.* **1982**, *44*, 83–126; b) E. H. Yonemoto, R. L. Riley, Y. L. Kim, S. J. Atherton, R. H. Schmehl, T. E. Mallouk, *J. Am. Chem. Soc.* **1992**, *114*, 8081–8087; c) V. Schild, D. van Loyen, H. Dürr, H. Bouas-Laurent, C. Turro, M. Wörner, M. R. Pokhrel, S. H. Bossmann, *J. Phys. Chem. A* **2002**, *106*, 9149–9158; d) A. Slamaschwok, M. Ottolenghi, D. Avnir, *Nature* **1992**, *355*, 240–242; e) X. D. Wang, B. W. Zhang, J. W. Bai, Y. Cao, X. R. Xiao, J. M. Zhu, *J. Phys. Chem.* **1992**, *96*, 2886–2891; f) M. Seiler, H. Dürr, *Lei-*

bigs Ann. **1995**, 407–413; g) D. C. Craig, K. P. Ghiggino, K. A. Jolliffe, S. J. Langford, M. N. Paddon-Row, *J. Org. Chem.* **1997**, *62*, 2381–2386; h) Y.-Z. Hu, S. Tsukiji, S. Shinkai, S. Oishi, I. Hamachi, *J. Am. Chem. Soc.* **2000**, *122*, 241–253.

[4] a) *Photocatalysis*, (Eds.: M. Kaneko, I. Okura) Springer, Berlin, **2002**; b) D. C. Bookbinder, N. S. Lewis, M. S. Wrighton, *J. Am. Chem. Soc.* **1981**, *103*, 7656–7659; c) B. Steiger, L. Walder, *Helv. Chim. Acta* **1992**, *75*, 90–108; d) L. Hammarström, M. Almgren, T. Norby, *J. Phys. Chem.* **1992**, *96*, 5017–5024; e) S. V. Lymar, J. K. Hurst, *J. Am. Chem. Soc.* **1992**, *114*, 9498–9503; f) S. Kim, S. E. Yun, C. Kang, *J. Electroanal. Chem.* **1999**, *465*, 153–159; g) H. Tatsumi, K. Takagi, M. Fujita, K. Kano, T. Ikeda, *Anal. Chem.* **1999**, *71*, 1753–1759; h) M. E. Ghica, C. M. A. Brett, *Anal. Chim. Acta* **2005**, *532*, 145–151.

[5] S. Saha, J. F. Stoddart, *Chem. Soc. Rev.* **2007**, *36*, 77–92.

[6] a) R. A. Bissell, E. Cordova, A. E. Kaifer, J. F. Stoddart, *Nature* **1994**, *369*, 133–137; b) A. C. Benniston, A. Harriman, V. M. Lynch, *J. Am. Chem. Soc.* **1995**, *117*, 5275–5291; c) Y. Liu, A. H. Flood, P. A. Bonvallett, S. A. Vignon, B. H. Northrop, H. R. Tseng, J. O. Jeppesen, T. J. Huang, B. Brough, M. Baller, S. Magonov, S. D. Solares, W. A. Goddard, C. M. Ho, J. F. Stoddart, *J. Am. Chem. Soc.* **2005**, *127*, 9745–9759.

[7] a) P. R. Ashton, R. Ballardini, V. Balzani, I. Baxter, A. Credi, M. C. T. Fyfe, M. T. Gandolfi, M. Gomez-Lopez, M. V. Martinez-Diaz, A. Piersanti, N. Spencer, J. F. Stoddart, M. Venturi, A. J. P. White, D. J. Williams, *J. Am. Chem. Soc.* **1998**, *120*, 11932–11942; b) A. C. Benniston, P. R. Mackie, A. Harriman, *Angew. Chem.* **1998**, *110*, 376–378; c) S. A. Vignon, J. F. Stoddart, *Collect. Czech. Chem. Commun.* **2005**, *70*, 1493–1576.

[8] a) A. C. Benniston, A. Harriman, *J. Am. Chem. Soc.* **1994**, *116*, 11531–11537; b) F. M. Raymo, J. F. Stoddart, *Pure Appl. Chem.* **1996**, *68*, 313–322; c) P. L. Anelli, P. R. Ashton, R. Ballardini, V. Balzani, M. Delgado, M. T. Gandolfi, T. T. Goodnow, A. E. Kaifer, D. Philp, M. Pietraszkiewicz, L. Prodi, M. V. Reddington, A. M. W. Slawin, N. Spencer, J. F. Stoddart, C. Vicent, D. J. Williams, *J. Am. Chem. Soc.* **1992**, *114*, 193–218.

[9] L. Michaelis, E. S. Hill, *J. Gen. Physiol.* **1933**, *16*, 859–866.

[10] C. L. Bird, A. T. Kuhn, *Chem. Soc. Rev.* **1981**, *10*, 49–82.

[11] T. M. Bockman, J. K. Kochi, *J. Org. Chem.* **1990**, *55*, 4127–4135.

[12] a) P. Wardman, *J. Phys. Chem. Ref. Data* **1989**, *18*, 1637–1755; b) R. P. Thummel, F. Lefoulon, S. Chirayil, V. Goulle, *J. Org. Chem.* **1988**, *53*, 4745–4747.

[13] a) A. C. Benniston, A. Harriman, P. Y. Li, C. A. Sams, M. D. Ward, *J. Am. Chem. Soc.* **2004**, *126*, 13630–13631; b) A. C. Benniston, A. Harriman, P. Y. Li, P. V. Patel, J. P. Rostron, C. A. Sams, *J. Phys. Chem. A* **2006**, *110*, 9880–9886.

[14] a) J. Bonvoison, J. P. Launay, W. Werbouwe, M. van der Auweraer, F. C. de Schryver, *J. Phys. Chem.* **1996**, *100*, 17079–17082; b) A. Heckmann, S. Amthor, C. Lambert, *Chem. Commun.* **2006**, 2959–2961; c) J. C. Lacroix, K. I. Chane-Ching, F. Maquère, F. Maurel, *J. Am. Chem. Soc.* **2006**, *128*, 7264–7276; d) S. Dümmler, W. Roth, I. Fischer, A. Heckmann, C. Lambert, *Chem. Phys. Lett.* **2005**, *408*, 264–268; e) F. Dumar, N. Gautier, N. Gallego-Planas, Y. Sahin, E. Levillain, N. Mercier, P. Hudhomme, M. Masino, A. Girlando, V. Lloveras, J. Vidal-Gancedo, C. Rovira, *J. Org. Chem.* **2004**, *69*, 2164–2177.

[15] A. C. Benniston, A. Harriman, P. Y. Li, P. V. Patel, C. A. Sams, *Phys. Chem. Chem. Phys.* **2005**, *7*, 3677–3679.

[16] A. C. Benniston, A. Harriman, P. Y. Li, J. P. Rostron, *Tetrahedron Lett.* **2005**, *46*, 7291–7293.

[17] W. L. F. Armarego, C. L. L. Chai, *Purification of Laboratory Chemicals*, 5th ed., Butterworth–Heinemann, London, **2003**.

[18] M. Griffin, A. Muys, C. Noble, D. Wang, C. Eldershaw, K. E. Gates, K. Burrage, G. R. Hanson, *Mol. Phys. Rep.* **1999**, *26*, 60–84.

[19] Gaussian 03, Revision C.02, M. J. Frisch, G. W. Trucks, H. B. Schlegel, G. E. Scuseria, M. A. Robb, J. R. Cheeseman, J. A. Montgomery, Jr., T. Vreven, K. N. Kudin, J. C. Burant, J. M. Millam, S. S. Iyengar, J. Tomasi, V. Barone, B. Mennucci, M. Cossi, G. Scalmani, N. Rega, G. A. Petersson, H. Nakatsuji, M. Hada, M. Ehara, K. Toyota, R. Fukuda, J. Hasegawa, M. Ishida, T. Nakajima, Y. Honda, O. Kitao, H. Nakai, M. Klene, X. Li, J. E. Knox, H. P. Hratchian, J. B. Cross, V. Bakken, C. Adamo, J. Jaramillo, R. Gomperts, R. E. Stratmann, O. Yazyev, A. J. Austin, R. Cammi, C. Pomelli, J. W. Ochterski, P. Y. Ayala, K. Morokuma, G. A. Voth, P. Salvador, J. J. Dannenberg, V. G. Zakrzewski, S. Dapprich, A. D. Daniels, M. C. Strain, O. Farkas, D. K. Malick, A. D. Rabuck, K. Raghavachari, J. B. Foresman, J. V. Ortiz, Q. Cui, A. G. Baboul, S. Clifford, J. Cioslowski, B. B. Stefanov, G. Liu, A. Liashenko, P. Piskorz, I. Komaromi, R. L. Martin, D. J. Fox, T. Keith, M. A. Al-Laham, C. Y. Peng, A. Nanayakkara, M. Challacombe, P. M. W. Gill, B. Johnson, W. Chen, M. W. Wong, C. Gonzalez, J. A. Pople, Gaussian, Inc., Wallingford CT, **2004**.

[20] a) M. Cossi, V. Barone, R. Cammi, J. Tomasi, *Chem. Phys. Lett.* **1996**, *255*, 327–335; b) M. Cossi, V. Barone, B. Mennucci, J. Tomasi, *Chem. Phys. Lett.* **1998**, *286*, 253–260; c) J. B. Foreman, T. A. Keith, K. B. Wiberg, J. Snoonian, M. J. Frisch, *J. Phys. Chem.* **1996**, *100*, 16098–16104.

[21] B. R. Brooks, R. E. Bruccoleri, B. D. Olafson, D. J. States, S. Swaminathan, M. Karplus, *J. Comp. Chem.* 1983, 4, 187–217.

[22] J. Rebek Jr, T. Costello, R. Wattley, *J. Am. Chem. Soc.* **1985**, *107*, 7487–7493.

[23] A. Sleegers, E. V. Dehmlow, *Leibigs Ann. Chem.* **1992**, 953–959.

[24] P. D. Beer, Z. Chen, A. Grieve, J. Haggitt, *J. Chem. Soc Chem. Commun.* **1994**, 2413–2414.

[25] J. Hassan, M. Sévignon, C. Gozzi, E. Schulz, M. Lemaire, *Chem. Rev.* **2002**, *102*, 1359–1470.

[26] a) M. Castella-Ventura, E. Kassab, *J. Raman Spectrosc.* **1998**, *29*, 511–536; b) L. Ould-Moussa, O. Poizat, M. Castella-Ventura, G. Buntinx, E. Kassab, *J. Phys. Chem.* **1996**, *100*, 2072–2082; c) H.-J. Hofmann, R. Cimiraglia, J. Tomasi, *J. Mol. Struct. (THEOCHEM)* **1986**, *139*, 213–219; d) T. Ishida, M. Murakami, G. Watanabe, H. Yoshikawa, S. Nishikori, *Internet Electron. J. Mol. Des.* **2003**, *2*, 14–23.

[27] H. Wolkers, R. Stegmann, G. Grenking, K. Dehnicke, D. Frenske, G. Baum, *Z. Naturforsch. B* **1993**, *48*, 1341–1347.

[28] A. Dzyabchenko, H. A. Scheraga, *Acta. Crystallogr. Sect. B* **2004**, *60*, 228–237.

[29] a) D. Becke, *J. Chem. Phys.* **1993**, *98*, 5648–5652; b) C. T. Lee, W. E. Yang, R. G. Parr, *Phys. Rev. B* **1988**, *37*, 785–789; c) M. J. Frisch, J. A. Pople, J. S. Binkley, *J. Chem. Phys.* **1984**, *80*, 3265–3269.

[30] B. D. Allen, A. C. Benniston, A. Harriman, I. Llarena, C. A. Sams, *J. Phys. Chem. A* **2007**, *111*, 2641–2649.

[31] Y. Huang. J. B. Hopkins, *J. Phys. Chem.* **1996**, *100*, 9585–9590.

[32] C. Pratt Brock, *J. Res. Natl. Inst. Stand. Technol.* **1996**, *101*, 321–325.

[33] a) P. M. S. Monk, N. M. Hodkinson, S. A. Ramzan, *Dyes Pigm.* **1999**, *43*, 207–217; b) W. W. Porter, T. P. Vaid, *J. Org. Chem.* **2005**, *70*, 5028–5035; c) P. M. S. Monk, R. D. Fairweather, M. D. Ingram, J. A. Duffy, *J. Chem. Soc. Perkin Trans. 2* **1992**, 2039–2041.

[34] a) E. M. Kosower, J. L. Cotter, *J. Am. Chem. Soc.* **1964**, *86*, 5524–5530; b) C. S. Johnson, H. S. Gutowsky, *J. Chem. Phys.* **1963**, *39*, 58–62; c) D. Guerin-Ouler, C. Nicollin, C. Sierro, C. Lamy, *Mol. Phys.* **1977**, *34*, 161–170; d) D. W. Clack, J. C. Evans, A. Y. Obad, C. C. Rowlands, *Tetrahedron* **1983**, *39*, 2615–3620. D. W. Clack, J. C. Evans, C. R. Morris, C. C. Rowlands, *Chem. Phys. Lett.* **1985**, *118*, 55–59.

[35] N. S. Sariciftci, A. Werner, M. Mehring, *Mol. Phys.* **1992**, *75*, 1269–1274.

[36] D. J. Barker, R. P. Cooney, L. A. Summers, *J. Raman Spectrosc.* **2005**, *16*, 265–271.

[37] a) F. Bruin, F. W. Heineken, M. Bruin, A. Zahlen, *J. Chem. Phys.* **1962**, *36*, 2783–2788; b) C. S. Johnson, R. E. Visco, H. S. Gutowsky, A. M. Hartley, *J. Chem. Phys.* **1962**, *37*, 1580–1584; c) N. S. Sariciftci, A. Werner, A. Grupp, M. Mehring, G. Götz, P. Bäuerle, F. Effenberger, *Mol. Phys.* **1992**, *75*, 1259–1267; d) D. W. Clack, J. C. Evans, A. Y. Obaid, C. C. Rowlands, *J. Chem. Soc. Perkin Trans. 2* **1985**, 1653–1657; e) A. Funston, J. P. Kirby, J. R. Miller, L. Pospisil, J. Fiedler, M. Hromadova, M. Gal, J. Pecka, M. Valasek, Z. Zawada, P. Rempala, J. Michl, *J. Phys. Chem. A* **2005**, *109*, 10862–10869.

[38] L. M. Stock, M. R. Wasielewski, *J. Am. Chem. Soc.* **1977**, *99*, 50–59.
[39] H. M. McConnell, *J. Chem. Phys.* **1956**, *24*, 764–768.
[40] a) C. S. Johnson, H. S. Gutowsky, *J. Chem. Phys.* **1963**, *39*, 58–62; b) A. D. McLachlan, *Mol. Phys.* **1958**, *1*, 233–237.

Received: June 8, 2007
Published online: August 23, 2007

